International Journal of Nanomedicine

Dovepress
open access to scientific and medical research

Open Access Full Text Article

ORIGINAL RESEARCH

^{131}I-labeled polyethylenimine-entrapped gold nanoparticles for targeted tumor SPECT/CT imaging and radionuclide therapy

This article was published in the following Dove Press journal:
International Journal of Nanomedicine

Na Sun[1,*]
Lingzhou Zhao[1,*]
Jingyi Zhu[2,*]
Yujie Li[1]
Ningning Song[1]
Yan Xing[1]
Wenli Qiao[1]
He Huang[2]
Jinhua Zhao[1]

[1]Department of Nuclear Medicine, Shanghai General Hospital, Shanghai Jiao Tong University School of Medicine, Shanghai 200080, People's Republic of China; [2]State Key Laboratory of Material-Oriented Chemical Engineering, School of Pharmaceutical Sciences, Nanjing Tech University, Nanjing 211816, People's Republic of China

*These authors contributed equally to this work

Purpose: Polyethylenimine (PEI) has been widely used as a versatile template to develop multifunctional nanosystems for disease diagnosis and treatment. In this study, we manufactured iodine-131 (^{131}I)-labeled PEI-entrapped gold nanoparticles (Au PENPs) as a novel nanoprobe for single-photon emission computed tomography/computed tomography (SPECT/CT) imaging and radionuclide therapy.

Materials and methods: PEI was PEGylated and sequentially conjugated with Buthus martensii Karsch chlorotoxin (BmK CT, a tumor-specific ligand which can selectively bind to MMP2), 3-(4′-hydroxyphenyl)propionic acid-OSu (HPAO), and fluorescein isothiocyanate to form the multifunctional PEI template for entrapment of Au NPs. Then, the PEI surface was radiolabeled with ^{131}I via HPAO to produce the novel nanoprobe (BmK CT-Au PENPs-^{131}I).

Results: The synthesized multifunctional Au PENPs before and after ^{131}I radiolabeling were well-characterized as follows: structure, X-ray attenuation coefficient, colloid stability, cytocompatibility, and radiochemical stability in vitro. Furthermore, BmK CT-Au PENPs-^{131}I were suitable for targeted SPECT/CT imaging and radionuclide therapy of tumor cells in vitro and in a xenograft tumor model in vivo.

Conclusion: The developed multifunctional Au PENPs are a promising theranostic platform for targeted imaging and treatment of different MMP2-overexpressing tumors.

Keywords: polyethylenimine, BmK CT, gold nanoparticles, SPECT/CT imaging, radionuclide therapy

Correspondence: He Huang
State Key Laboratory of Material-Oriented Chemical Engineering, School of Pharmaceutical Sciences, Nanjing Tech University, Nanjing 211816, People's Republic of China
Tel +86 255 813 9942
Fax +86 255 813 9942
Email huangh@njtech.edu.cn

Jinhua Zhao
Department of Nuclear Medicine, Shanghai General Hospital, Shanghai Jiao Tong University School of Medicine, Shanghai 200080, People's Republic of China
Tel +86 213 779 8352
Fax +86 213 779 8352
Email zhaojinhua1963@126.com

Introduction

Nanomedicine holds great promise for diagnosis and treatment of various diseases, particularly cancer.[1,2] Glioma is the most common intracranial tumor and has the highest mortality rate.[3] Due to the invasive nature of glioma cells, difficulties in accurate delineation of tumor margin and unsatisfactory treatment result in increased mortality.[4,5] For high grade gliomas, the 5-year survival rate is less than 5%.[6] Thus, it is urgent to develop novel diagnostic and therapeutic options. Rapid development of nanomedicines has conferred the advantages of different imaging modalities and therapy techniques against this malignant disease.[7]

Nuclear medicine is a powerful technology that uses radionuclides for diagnosis and treatment of many diseases.[8–10] Single-photon emission computed tomography (SPECT), one of the most important radionuclide-based imaging techniques, has shown great value in tumor imaging.[11–14] Meanwhile, a number of therapeutic

submit your manuscript | www.dovepress.com
DovePress
http://doi.org/10.2147/IJN.S203259

radionuclides have been widely used for tumor treatment, including but not limited to iodine-131 (^{131}I), rhenium-188 (^{188}Re), yttrium-90 (^{90}Y), lutetium-177 (^{177}Lu), and radium-223 (^{223}Ra).[15–21] Among these therapeutic radionuclides, ^{131}I has been routinely used in radionuclide therapy and imaging of thyroid diseases, such as thyroid cancer, because of its high affinity for the thyroid and relatively long half-life (8.01 days). Beta minus decay provides therapeutic effects, while gamma emissions are used for SPECT imaging.[17,22,23] Therefore, ^{131}I-labeled molecular probes have been developed for theranostic applications in treatment of various kinds of cancer.[24–27] Several studies have suggested that ^{131}I-labeled glioma-targeting ligands such as chlorotoxin, and chlorotoxin-like peptides such as Buthus martensii Karsch chlorotoxin (BmK CT), are potential candidates for targeted SPECT imaging and radionuclide therapy of glioma.[28–31] To overcome the main obstacle of blood–brain barrier (BBB), some interventional therapy strategies have been attempted, which have greatly promoted the development of glioma treatment.[32]

Computed tomography (CT) is a powerful, non-invasive diagnostic technique that frequently requires additional CT contrast agents for high resolution imaging to allow for more accurate diagnoses. However, commonly-used iodine-based CT contrast agents have short half-lives and poor specificity.[28,33] Recent studies evaluating gold nanoparticles (Au NPs) have shown that various Au-based CT contrast agents are emerging due to high atomic number, tunable surface chemical modification chemistry, and biocompatibility after appropriate surface modifications.[34–37] Polyethylenimine (PEI) has the advantages of high-density amines and good water solubility, and it has been widely used as a template to produce multifunctional CT imaging agents.[38–40] PEI-entrapped Au NPs (Au PENPs) can be easily PEGylated and functionalized with targeting molecules, resulting in prolonged blood circulation time, low toxicity, and designed targeting ability for imaging applications. In addition, PEI has been identified as an excellent vehicle to encapsulate drugs or genes for treatment of different cancers, suggesting that PEI is an excellent template for development of theranostic nanosystems.[41–43] Our previous work has demonstrated that PEGylated PEI was able to load Au NPs and doxorubicin for tumor-targeted CT imaging and chemotherapy.[44] Furthermore, these Au NPs could be readily labeled with radionuclides for nuclear medicine applications. For instance, we have shown that PEI could be utilized to entrap Au NPs, then labeled with ^{99m}Tc for SPECT/CT imaging of tumors.[45,46] However, few studies have evaluated the use of PEI as a vehicle to load therapeutic radionuclides for tumor treatment.

The previous successes and properties of ^{131}I suggest that PEI may be further utilized as a versatile platform to develop multifunctional nanoprobes for tumor theranostic applications. In this work, we reported the development of ^{131}I-labeled Au PENPs modified with the glioma-targeting peptide BmK CT for targeted SPECT/CT imaging and radionuclide therapy of glioma. First, PEI was sequentially modified with BmK CT via a PEG linker. Carboxyl-terminated methoxy PEG (*m*PEG-COOH), 3-(4′-hydroxyphenyl)propionic acid-OSu (HPAO), and fluorescein isothiocyanate (FI) were used to form the multifunctional PEI template. The template was used to entrap Au NPs via sodium borohydride reduction chemistry. Then, the remaining terminal amines were acetylated by acetic oxide (Ac_2O), and the product was radiolabeled with ^{131}I via HPAO, resulting in {$(Au^0)_{200}$-PEI.NHAc-*m*PEG-(PEG-BmK CT)-^{131}I-HPAO-FI} PENPs (BmK CT-Au PENPs-^{131}I). The multifunctional Au PENPs before and after ^{131}I labeling were well-characterized, including structure, X-ray attenuation coefficient, colloidal stability under different pH and temperature conditions, cytocompatibility at an Au concentration up to 200 μM, and radiochemical stability in vitro. Furthermore, the prepared BmK CT-Au PENPs-^{131}I could be utilized for targeted SPECT/CT imaging and radionuclide therapy of glioma cells in vitro and in a xenograft tumor model in vivo. The developed multifunctional Au PENPs may provide a promising theranostic platform for targeted imaging and radionuclide therapy of glioma.

Materials and methods

Materials

BmK CT peptide with a cysteine at its C-terminal was synthesized by Shanghai Bootech BioScience & Technology Co., Ltd. (Shanghai, People's Republic of China). Maleimide-PEG-succinimidyl valerate (MAL-PEG-SVA, Mw =5,000) and *m*PEG-COOH (Mw =5,000) were supplied by Shanghai Yanyi Biotechnology Corporation (Shanghai, People's Republic of China). Na^{131}I solution was provided by Shanghai GMS Pharmaceutical Co., Ltd (Shanghai, People's Republic of China). Branched PEI (Mw =25,000), $HAuCl_4$, DMSO, sodium borohydride ($NaBH_4$), HPAO, 1-butanethiol, 1-ethyl-3-(3-dimethylaminopropyl) carbodiimide hydrochloride (EDC), chloramine-T trihydrate

(ch-T), potassium iodide (KI), triethylamine (TEA), and all other chemicals and solvents were purchased from Sigma-Aldrich Co. (St Louis, MO, USA). Disposable PD-10 desalting columns were obtained from GE Pharmacia (GE Inc., Fairfield, CT, USA). FBS, DMEM, DAPI, and Cell Counting Kit-8 (CCK-8) were provided by Hangzhou Jinuo Biomedical Technology (Hangzhou, People's Republic of China). Regenerated cellulose dialysis membranes (molecular weight cutoff [MWCO] =14,000 and 1,000) were purchased from Fisher (Pittsburgh, PA, USA). C6 cells (a rat glioma cell line) were obtained from the Chinese Academy of Sciences (Shanghai, People's Republic of China). Six-week old BALB/c nude mice were purchased from Shanghai Slac Laboratory Animal Center, and animal experiments in this study were approved by the ethics committee and strictly performed according to standard procedures.

Synthesis of BmK CT-Au PENPs-^{131}I

BmK CT-modified PEI was synthesized according to our previous work.[29] Briefly, *m*PEG-COOH (300 mg) dissolved in DMSO was activated by EDC (175.2 mg), then added dropwise into a DMSO solution containing PEI.NH_2 (100.0 mg) with vigorous stirring for 3 days at room temperature to obtain PEI.NH_2-*m*PEG. MAL-PEG-SVA (300.0 mg) dissolved in DMSO was mixed with the reaction solution for another 3 days to form PEI.NH_2-*m*PEG-(PEG-MAL). BmK CT (114.8 mg) was reacted with the MAL groups of PEI overnight to produce PEI.NH_2-*m*PEG-(PEG-BmK CT). Unreacted MAL groups on the PEI surface were blocked using excess 1-butanethiol to prevent reaction with HPAO in the following step. After that, HPAO (31.6 mg) and FI (7.8 mg) were sequentially added to the reaction mixture with stirring overnight to obtain PEI.NH_2-*m*PEG-(PEG-BmK CT)-HPAO-FI.

Functionalized PEI was used as a template for entrapment of Au NPs using sodium borohydride reduction chemistry with a PEI/Au salt molar ratio of 1:200. Briefly, an aqueous $HAuCl_4$ solution (0.01 M, 80 mL) was mixed with the PEI.NH_2-*m*PEG-(PEG-BmK CT)-HPAO-FI (768.5 mg, 20 mL) solution by stirring for 0.5 hours. Then, cold $NaBH_4$ solution (10.0 mg/mL, 9.1 mL) was added rapidly and the mixture was stirred for 2 hours to form {$(Au^0)_{200}$-PEI.NH_2-*m*PEG-(PEG-BmK CT)-HPAO-FI} NPs. After acetylation of the remaining NH_2 groups on the surface of PEI by reacting with TEA (1,957.1 μL) and Ac_2O (1,107.6 μL) for 24 hours, the mixture was purified using a dialysis membrane (MWCO =14,000) against PBS (three times, 2 L) and water (six times, 2 L) over 3 days to remove excess reactants and byproducts. The final {$(Au^0)_{200}$-PEI.NHAc-*m*PEG-(PEG-BmK CT)-HPAO-FI} NPs (BmK CT-Au PENPs) were obtained by lyophilization. For comparison, Au PENPs without BmK CT modification were also prepared under similar conditions. The intermediate products were collected, purified, and characterized to calculate the average number of conjugated moieties (HPAO, BmK CT, *m*PEG, and FI) per PEI.

Finally, ^{131}I radiolabeling of BmK CT-Au PENPs was achieved using the chloramine T method. Briefly, a PBS solution of BmK CT-Au PENPs (200 μg, 200 μL) was mixed with chloramine T (200 μg) and Na^{131}I solution (20 mCi, 200 μL). After incubation for 30 minutes at 37°C under continuous stirring, the reaction mixture was eluted through PD-10 desalting columns with PBS as the mobile phase, and 1 mL of liquid was collected in each tube. After ten tubes were collected, the radioactivity of each tube was measured. The radiochemical yield was calculated as (A0-A)/A0. A0 is the total activity of ^{131}I in the reaction, and A is the activity of PD-10 desalting column after purification. BmK CT-Au PENPs-^{131}I was collected and Au PENPs-^{131}I without BmK CT was also prepared for comparison using the same method. Radiochemical purity and radiostability were assessed in vitro according to our previous work.[17]

Characterization techniques

^{1}H NMR spectra of samples dissolved in D_2O were obtained using a Bruker AV400 nuclear magnetic resonance spectrometer (Bruker AXS Advanced X-ray Solutions GmbH, Karlsruhe, Germany). UV-Vis spectra were collected using a Lambda 25 UV-Vis spectrophotometer (PerkinElmer, Inc., Waltham, MA, USA). Dynamic light scattering (DLS) and zeta potential were measured using a Malvern Zetasizer Nano ZS model ZEN 3600 (Malvern Instruments, Malvern, UK) with a standard 633 nm laser. The Au content of the prepared Au NPs was evaluated using a Leeman Prodigy inductively coupled plasma optical emission spectrometer (Teledyne Leeman Labs, Hudson, NH, USA). Transmission electron microscopy (TEM) samples were prepared by dropping an aqueous particle suspension (1 mg/mL) onto a carbon-coated copper grid, followed by air-drying prior to analysis. TEM imaging was performed using a JEOL 2010F analytical electron microscope (JEOL, Tokyo, Japan) at an operating voltage of 200 kV. The X-ray attenuation properties of the

formed Au NPs were compared using Omnipaque (iohexol 300; GE Healthcare, Chicago, IL, USA) at different Au or iodine concentrations (6.25–100 μM). CT images were acquired using a GE Discovery STE PET/CT system (GE Healthcare) with the following settings: 100 kV, 220 mA, and a slice thickness of 1.25 mm. SPECT imaging was performed using a GE Infinia SPECT scanner equipped with an Xeleris workstation and High-Energy General-Purpose collimators (GE Healthcare).

Cell culture and construction of glioma-bearing nude mouse model

C6 cells were cultured in DMEM containing 10% FBS in a humidified incubator with 5% CO_2 at 37°C. We established a subcutaneous glioma model in nude mice for in vivo experiments. Briefly, 2×10^6 C6 cells were subcutaneously injected in the right flank of each mouse. The mice were then fed regularly for 3 weeks and tumor volumes reached 0.8–1.0 cm^3.

Cytotoxicity assay

CCK-8 assay was used to assess the cytotoxicity of BmK CT-Au PENPs before and after ^{131}I labeling in C6 cells. In brief, C6 cells in the logarithmic growth phase were seeded onto a 96-well plate (1×10^4 cells per well) and incubated overnight. The cells were treated with Au PENPs or BmK CT-Au PENPs at different final Au concentrations (0, 12.5, 25, 50, 100, and 200 μM, respectively). After 24 hours' incubation, C6 cell viability of each group was analyzed using the CCK-8 method according to standard procedures. Cytotoxicity of BmK CT-Au PENPs-^{131}I in C6 cells was also evaluated at different radioactivity concentrations (0, 12.5, 25, 50, 100, and 200 μCi/mL, respectively). After 24 hours' incubation, the viability of C6 cells was determined.

In vitro targeting assay

Flow cytometry and confocal microscopy were used to assess the targeting efficiency of BmK CT-Au PENPs to tumor cells in vitro. For flow cytometry analysis, C6 cells in the logarithmic growth phase were seeded onto a 6-well plate (2×10^5 cells per well) and incubated overnight. The cells were treated with BmK CT-Au PENPs or Au PENPs at final Au concentrations of 0.5 μM and 5 μM, respectively. PBS was used as the control. After 4 hours' incubation, the cells were trypsinized, centrifuged, and resuspended in PBS. The mean fluorescence intensity of approximately 10,000 cells in each group was analyzed using a BD AccuriTM C6 Flow Cytometer in the FL1-fluorescence channel.

For confocal microscopy imaging, C6 cells in the logarithmic growth phase (5×10^4) were seeded onto 35 mm glass bottom dishes and incubated overnight. The cells were treated with BmK CT-Au PENPs or Au PENPs at a final Au concentration of 5 μM. PBS was used as the control. After culturing for 4 hours, the cells were rinsed with PBS, fixed with 4% paraformaldehyde and nucleic acids were stained with DAPI according to standard procedures. FL1-fluorescence of the stained cells was measured at 488 nm by confocal microscopy (LSM 700, Carl Zeiss Meditec AG, Jena, Germany).

SPECT and CT imaging in vitro

Feasibility of BmK CT-Au PENPs for CT imaging of tumor cells was assessed in vitro. First, C6 cells in the logarithmic growth phase were seeded onto a 6-well plate (2×10^5 cells per well) and incubated for 24 hours. The cells were treated with BmK CT-Au PENPs or Au PENPs at different Au concentrations (20, 40, 60, 80, and 100 μM, respectively). After 4 hours' incubation, the cells were trypsinized, centrifuged, and rinsed with PBS in 1.5 mL microcentrifuge tubes, then imaged using a CT system (GE Inc., USA).

After ^{131}I radiolabeling, the tumor-targeted SPECT imaging capability of BmK CT-Au PENPs-^{131}I was evaluated in vitro using a similar method. C6 cells were incubated, then treated with BmK CT-Au PENPs-^{131}I or Au PENPs-^{131}I at different radioactivity concentrations (0, 25, 50, 100, 200, and 400 μCi/mL). After 4 hours' incubation, the cells were trypsinized, centrifuged, rinsed, and imaged using an Infinia SPECT scanner.

SPECT and CT imaging in vivo

All animal experiments in this study were approved by the ethics committee of Shanghai General Hospital and conformed to the National Institutes of Health Guidelines. Before in vivo imaging, the glioma-bearing nude mice were randomly divided into two groups (five mice per group) and anesthetized with pentobarbital sodium (40 mg/kg). The mice were intravenously injected with PBS solutions containing BmK CT-Au PENPs or Au PENPs ([Au]=100 μM, 100 μL) to evaluate CT imaging performance in vivo. CT images were obtained at 0, 0.5, 2, 4, 6, 8, and 16 hours post-injection. For SPECT imaging, glioma-bearing nude mice were fed and given water

containing 1% potassium iodide for 3 days to block thyroid uptake of ^{131}I. Then, the mice were anesthetized and randomly divided into two groups (five mice per group). We intravenously injected a PBS solution of BmK CT-Au PENPs-^{131}I or Au PENPs-^{131}I at the same dose (500 μCi, 100 μL) into the mice and performed SPECT imaging at 0.5, 2, 4, 6, 8, and 16 hours post-injection using an Infinia SPECT scanner.

In vivo antitumor efficacy

The in vivo therapeutic efficacy of BmK CT-Au PENPs-^{131}I was further assessed in a subcutaneous tumor model. To reduce thyroid uptake of ^{131}I, the tumor-bearing nude mice were fed and given water containing 1% potassium iodide for 3 days. After being divided into five groups randomly (five mice per group), the mice in each group were intravenously injected with 100 μL PBS solutions of BmK CT-Au PENPs-^{131}I (250 μCi), Au PENPs-^{131}I (250 μCi), BmK CT-Au PENPs (0.1 M Au), or Au PENPs (0.1 M Au), or saline. Treatment was administered every 3 days for a total of seven treatments. During treatment, body weight and tumor size were recorded before each injection. After the 21-day treatment period, one mouse from each group was sacrificed to obtain the major organs (heart, liver, spleen, lung, and kidney) and the subcutaneous implanted tumors. The harvested major organs and tumors were stained with H&E according to the standard procedure. To further evaluate apoptosis in the treated glioma-bearing mice, the tumors were stained using the TUNEL method using an apoptosis detection kit (Hoffman'La Roche Ltd., Basel, Switzerland). The stained specimens were imaged using an AMEX 1200 inverted phase contrast microscope.

Statistical analysis

Experimental data in this study were analyzed by one-way ANOVA and the final data were marked with (*) for $p<0.05$, (**) for $p<0.01$, and (***) for $p<0.001$. A p-value <0.05 was considered statistically significant.

Results and discussion

Synthesis and characterization of the BmK CT-Au PENPs-^{131}I

PEGylation has been identified as an effective strategy to improve biocompatibility and pharmacokinetic properties of NPs. In our previous work, PEGylated PEI was successfully used as a template to entrap Au NPs for CT imaging or to encapsulate drugs for chemotherapy of tumors in -vivo.[41,44] In this study, PEGylated PEI was sequentially modified with BmK CT peptide using PEG linker, HPAO, and FI, and then utilized to entrap Au NPs. Remaining PEI surface amines were acetylated and the product was radiolabeled with ^{131}I via HPAO. The Au PENPs modified with BmK CT were used as a multifunctional nanoprobe for tumor-targeted SPECT/CT and radionuclide therapy (Figure 1). The intermediate products including PEI.NH_2-*m*PEG, PEI.NH_2-*m*PEG-(PEG-MAL), PEI.NH_2-*m*PEG -(PEG-BmK CT), PEI.NH_2-*m*PEG-(PEG-Bu)-HPAO, PEI.NH_2-*m*PEG-(PEG-BmK CT)-HPAO, PEI.NH_2-*m*PEG -(PEG-Bu)-HPAO-FI, and PEI.NH_2-*m*PEG-(PEG-BmK CT)-HPAO-FI, were characterized via ^{1}H NMR (Figure S1). The average number of *m*PEG, PEG, HPAO, BmK CT, and FI moieties attached to each PEI was estimated using NMR integration according to our previous work,[11,29] and the results were recorded in Table 1. Then, PEI.NH_2-*m*PEG-(PEG-BmK CT)-HPAO-FI and PEI.NH_2-*m*PEG-(PEG-Bu)-HPAO-FI were respectively employed as templates to entrap Au NPs for synthesis of BmK CT-Au PENPs and Au PENPs with an Au salt/PEI molar ratio of 200:1 as previously described.[11]

The synthetized Au NPs were analyzed with different techniques. Inductively coupled plasma optical emission-spectrometry was performed to calculate Au content, and the data indicated complete reduction of Au(III) to Au(0) in the BmK CT-Au PENPs and Au PENPs with the average numbers of Au atoms per PEI close to the selected Au salt/PEI molar ratio. Successful capture of Au NPs within PEI was confirmed by UV-Vis spectroscopy. In agreement with the results reported in the literature,[11] a noticeable surface plasmon resonance peak at approximately 540 nm was clearly observed due to the particle-induced light scattering effect (Figure S1).Furthermore, UV-Vis spectroscopy was used to assess stability of the Au NPs in vitro in the given pH (5.0–8.0) and temperature (4–50°C) ranges. As shown in Figure S2A and B, no obvious changes in absorption characteristics were observed in BmK CT-Au PENPs, indicating acceptable stability under different temperature and pH conditions. BmK CT-Au PENPs' particle size was measured using DLS and TEM. BmK CT-Au PENPs had a hydrodynamic diameter of 147.0±9.1 nm as determined by DLS, and Au core size of BmK CT-Au PENPs was 4.4 ±0.7 nm, as determined by TEM (Figure 2), smaller than the hydrodynamic size determined using DLS. This was likely due to the fact that TEM only measures the Au core of a single particle, rather than numerous Au NPs in

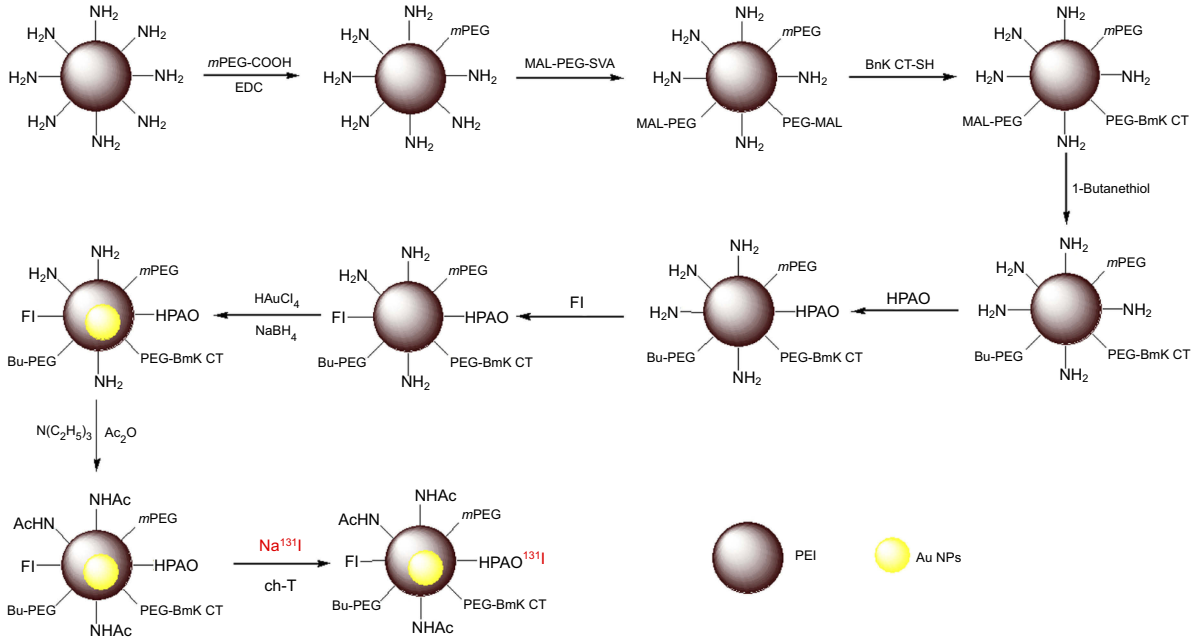

Figure 1 Preparation of BmK CT-Au PENPs-^{131}I.
Abbreviations: PEI, polyethylenimine; Au NPs, gold nanoparticles; *m*PEG-COOH, carboxyl-terminated methoxy PEG; EDC, 1-ethyl-3-(3-dimethylaminopropyl) carbodiimide hydrochloride; MAL-PEG-SVA, maleimide-PEG-succinimidyl valerate; BmK CT, Buthus martensii Karsch chlorotoxin; FI, fluorescein isothiocyanate; HPAO, 3-(4′-hydroxyphenyl)propionic acid-OSu; ch-T, chloramine-T trihydrate; BmKCT-Au PENPs-^{131}I, ^{131}I-labeled BmK CT modified polyethylenimine-entrapped gold nanoparticles; $NaBH_4$, sodium borohydride.

Table 1 The mean number of moieties attached to each PEI

	PEI.NH_2-*m*PEG-(PEG-BmK CT)-HPAO-FI	**PEI.NH_2-*m*PEG-(PEG-Bu)-HPAO-FI**
*m*PEG	13.3	
PEG	14.2	
BmK CT	4.8	0
HPAO	17.7	17.3
FI	5.4	5.7

Notes: PEI.NH_2 was first PEGylated using *m*PEG-COOH and conjugated with MAL-PEG-SVA to form PEI.NH_2-*m*PEG-(PEG-MAL). Then the PEI.NH_2-*m*PEG-(PEG-MAL) was divided in half. One was modified with BmK CT, and the other was reacted with 1-butanethiol. Therefore, the mean number of *m*PEG and PEG in PEI.NH_2-*m*PEG-(PEG-BmK CT)-HPAO-FI and PEI.NH_2-*m*PEG-(PEG-Bu)-HPAO-FI was the same.
Abbreviations: PEI, polyethylenimine; *m*PEG-COOH, carboxyl-terminated methoxy PEG; MAL-PEG-SVA, maleimide-PEG-succinimidyl valerate; BmK CT, Buthus martensii Karsch chlorotoxin; FI, fluorescein isothiocyanate; HPAO, 3-(4′-hydroxyphenyl)propionic acid-OSu.

aggregates, as measured by DLS. Notably, the low polydispersity index (0.3±0.06) determined using DLS and the relatively narrow size distribution determined using TEM, suggested favorable size uniformity of the BmK CT-Au PENPs. TEM also showed that BmK CT-Au PENPs were nearly spherical in shape, and high resolution TEM images further showed Au crystal lattices, suggesting high crystallinity of the formed BmK CT-Au PENPs (Figure 2C). This was confirmed through evaluation of selected area electron diffraction patterns, where the featured (111), (200), (220), and (311) rings were used to confirm the face-centered-cubic crystal structure (Figure 2D). Energy dispersive spectroscopy of BmK CT-Au PENPs samples indicates the existence and distribution of Au elements (Figure 2E). Finally, surface potentials of the BmK CT-Au PENPs and Au PENPs were estimated at 6.06±0.16 mV and 14.5±0.15 mV, respectively, demonstrating successful acetylation of the remaining surface amine groups of PEI.

The prepared Au NPs were readily labeled with ^{131}I using the chloramine-T method due to the presence of HPAO on the surface of PEI. The radiolabeling yields of BmK CT-Au PENPs-^{131}I and Au PENPs-^{131}I were 77.0 ±4.97% and 72.3±3.62% (n=3), respectively. After purification using a PD-10 column, the radiochemical purities were greater than 99%, and they remained above 90% after exposure to PBS at room temperature and FBS at 37ºC for 24 hours (Figure S2C and D), indicating excellent radiostability, which allowed for further in vitro and in vivo analyses.

Cytotoxicity assay

CCK-8 assay was used to assess the potential cytotoxicity of BmK CT-functionalized Au PENPs before and after ^{131}I radiolabeling (Figure S3). Viability of C6 cells treated with BmK CT-Au PENPs or Au PENPs

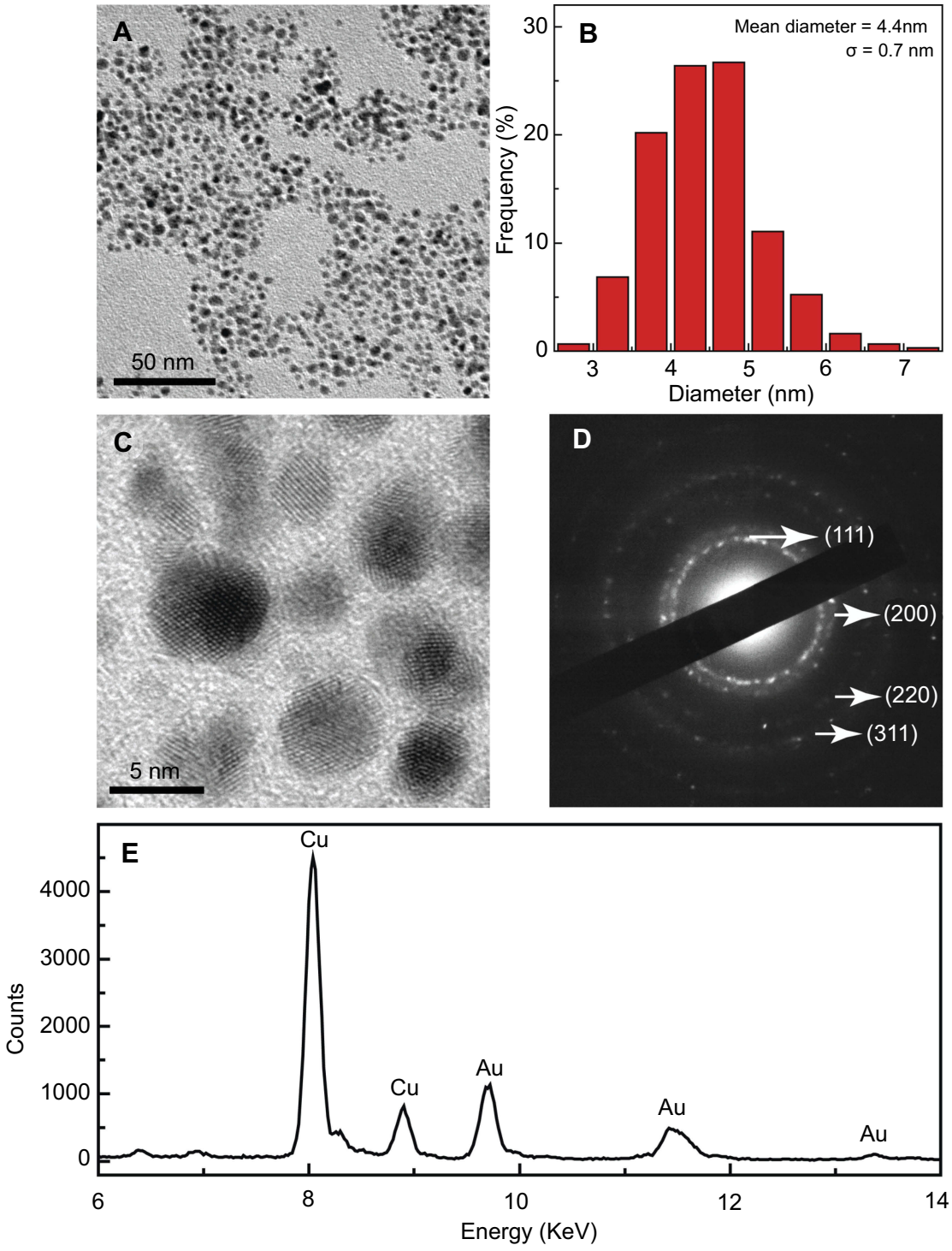

Figure 2 TEM image and size distribution of BmK CT-Au PENPs. (**A**) TEM image, (**B**) size distribution, (**C**) high-resolution TEM image, (**D**) selected area electron diffraction pattern, and (**E**) EDS spectrum of BmK CT-Au PENPs.
Abbreviations: TEM, transmission electron microscopy; BmK CT, Buthus martensii Karsch chlorotoxin; BmK CT-Au PENPs, BmK CT modified polyethylenimine-entrapped gold nanoparticles; EDS, energy dispersive spectroscopy.

remained high (>90%) at an Au concentration of up to 200 μM, similar to that observed in the PBS control group (Figure S3A). These results indicated that the BmK CT-Au PENPs prior to ^{131}I labeling were not cytotoxic to C6 cells in the given concentration range. In contrast, the viability of C6 cells gradually decreased with increased radioactivity concentration of the ^{131}I-labeled Au NPs (Figure S3B), and BmK CT-Au

PENPs-^{131}I exerted a stronger inhibitory effect compared with that of Au PENPs-^{131}I at the same radioactivity concentrations, demonstrating that the BmK CT modification enhanced cellular uptake of ^{131}I-labeled Au PENPs into C6 cells in the given concentration range.

Targeting specificity of the BmK CT-Au PENPs to tumor cells

BmK CT is a tumor-specific ligand and can selectively bind to MMP2 which is overexpressed in various tumors. Based on this property, BmK CT-Au PENPs were expected to specifically target C6 cells. Flow cytometry (Figure S4) and confocal microscopy (Figure S5) were used to assess targeting specificity of BmK CT-Au PENPs. Flow cytometry assay showed that the fluorescence intensity in C6 cells treated with BmK CT-Au PENPs for 4 hours was significantly higher than that in cells treated with untargeted Au PENPs at the same concentration ($p<0.05$). In contrast, the fluorescence intensity in C6 cells treated with Au PENPs was similar to that in the PBS control. These results demonstrated that the targeted ligand BmK CT increased uptake of Au PENPs into C6 cells. Similarly, enhanced cellular uptake of BmK CT-Au PENPs was visualized using confocal microscopy. After treatment with BmK CT-Au PENPs for 4 hours, C6 cells displayed prominent fluorescence signals, while cells treated with Au PENPs at the same concentration exhibited similar fluorescence signals to those of the PBS control, further confirming that uptake of BmK CT-Au PENPs in C6 cells was enhanced by modification with BmK CT. Thus, the synthetized BmK CT-Au PENPs displayed high targeting specificity to C6 cells based on flow cytometry and confocal microscopy analyses.

SPECT and CT imaging in vitro

SPECT and CT performance of BmK CT-Au PENPs were first evaluated in vitro (Figure 3). Due to high X-ray attenuation, Au NPs have been explored as contrast agents for CT imaging. In this study, the formed BmK CT-Au PENPs were compared with Omnipaque (a small molecule CT contrast agent used clinically) to investigate the effects of high X-ray attenuation on performance. As shown in Figure 3A–C, both Au NPs and Omnipaque had brighter CT images and higher HU values as their concentrations increased, while a sharper trend of Au NPs could be clearly seen as a result of larger HU values than Omnipaque at the same Au or I concentrations, revealing stronger X-ray attenuation by Au NPs than by iodine-based contrast agents. Similarly, for CT imaging in vitro, the brightness of CT images increased with increasing Au concentrations in the cells treated with BmK CT-Au PENPs and Au PENPs (Figure 3D and E). Quantitative analysis showed that a higher CT value was obtained in the C6 cells treated with BmK CT-Au PENPs than those treated with Au PENPs at Au concentrations of 20, 40, 60, 80, and 100 μM (Figure 3F). At an Au concentration of 100 μM, cells treated with BmK CT-Au PENPs showed a 2.2 times higher CT value than those treated with Au PENPs, indicating that BmK CT modification enhanced cellular uptake of Au PENPs into C6 cells.

SPECT images of C6 cells treated with BmK CT-Au PENPs-^{131}I were clearly brighter than those treated with Au PENPs-^{131}I at the same radioactivity concentrations (Figure 3G and H). Further quantitative analysis demonstrated that the radioactive signal intensity in the BmK CT-Au PENPs-^{131}I group was significantly higher than that in the Au PENPs-^{131}I group, especially at the radioactivity concentration of 400 μCi/mL (Figure 3I). These data indicated that BmK CT-Au PENPs-^{131}I allowed for excellent SPECT imaging of gliomas in vitro.

SPECT and CT imaging in vivo

The ^{131}I has been widely used in clinical radionuclide therapy. However, ^{131}I-labeled substances have some short-comings, such as low image resolution and in vivo dehalogenation. Therefore, before the in vivo experiments, all nude mice were fed with potassium iodide to saturate the thyroid and reduce the unwanted thyroid uptake of ^{131}I. SPECT and CT imaging suitability of BmK CT-Au PENPs-^{131}I was further evaluated in vivo in C6 tumor-bearing nude mice. As shown in Figure 4A, no obvious tumor SPECT signal was observed in mice after injection with BmK CT-Au PENPs-^{131}I or Au PENPs-^{131}I at 2 hours. However, tumor uptake in mice treated with BmK CT-Au PENPs-^{131}I gradually increased with time, and reached a peak at 8 hours post-injection and could be clearly visualized at 16 hours post-injection. In contrast, only a sight accumulation of radioactivity was observed in tumors treated with Au PENPs-^{131}I at 8 hours post-injection via the EPR effect, and no distinct tumor uptake was observed at other time points (Figure 4B), which was confirmed by the SPECT imaging of ex vivo tumors at 8 hours post-injection that showed

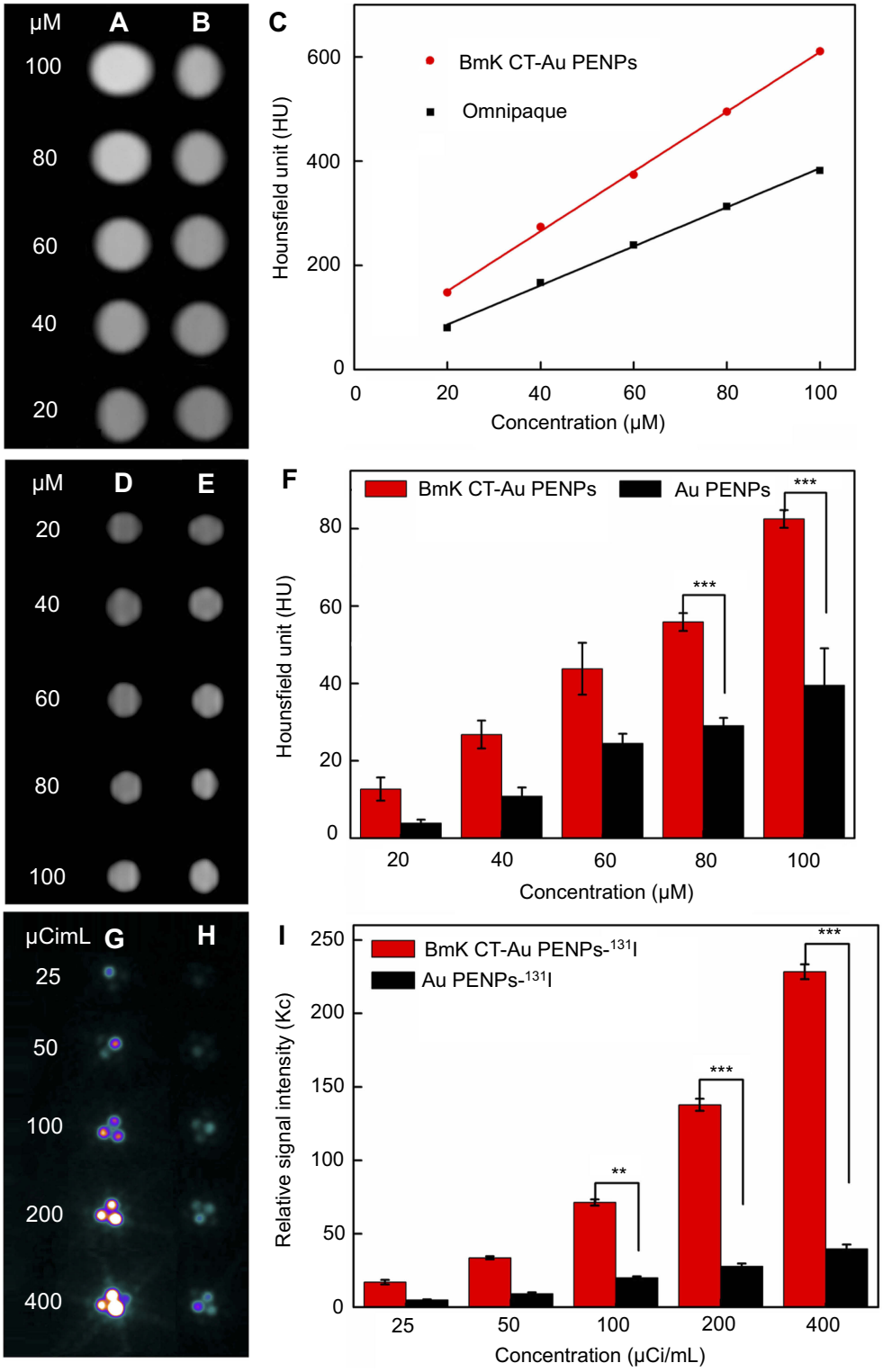

Figure 3 CT imaging of BmK CT-Au PENPs and SPECT imaging of BmK CT-Au PENPs-^{131}I in vitro. CT images of (**A**) BmK CT-Au PENPs and (**B**) Omnipaque at different Au or I concentrations, and (**C**) X-ray attenuation intensities. CT images of C6 cells treated with (**D**) Au PENPs or (**E**) BmK CT-Au PENPs for 4 hours at different Au concentrations, and (**F**) quantitative HU values. SPECT images of C6 cells treated with (**G**) Au PENPs-^{131}I or (**H**) BmK CT-Au PENPs-^{131}I for 4 hours at different radioactive concentrations, and (**I**) relative SPECT signal intensities. ** p<0.01, ***p<0.001

Abbreviations: CT, computed tomography; SPECT, single-photon emission computed tomography; BmK CT, Buthus martensii Karsch chlorotoxin; BmK CT-Au PENPs, BmK CT modified polyethylenimine-entrapped gold nanoparticles; Au PENPs, polyethylenimine-entrapped gold nanoparticles; BmK CT-Au PENPs-^{131}I, ^{131}I-labeled BmK CT modified polyethylenimine-entrapped gold nanoparticles; Au PENPs-^{131}I, ^{131}I-labeled polyethylenimine-entrapped gold nanoparticles.

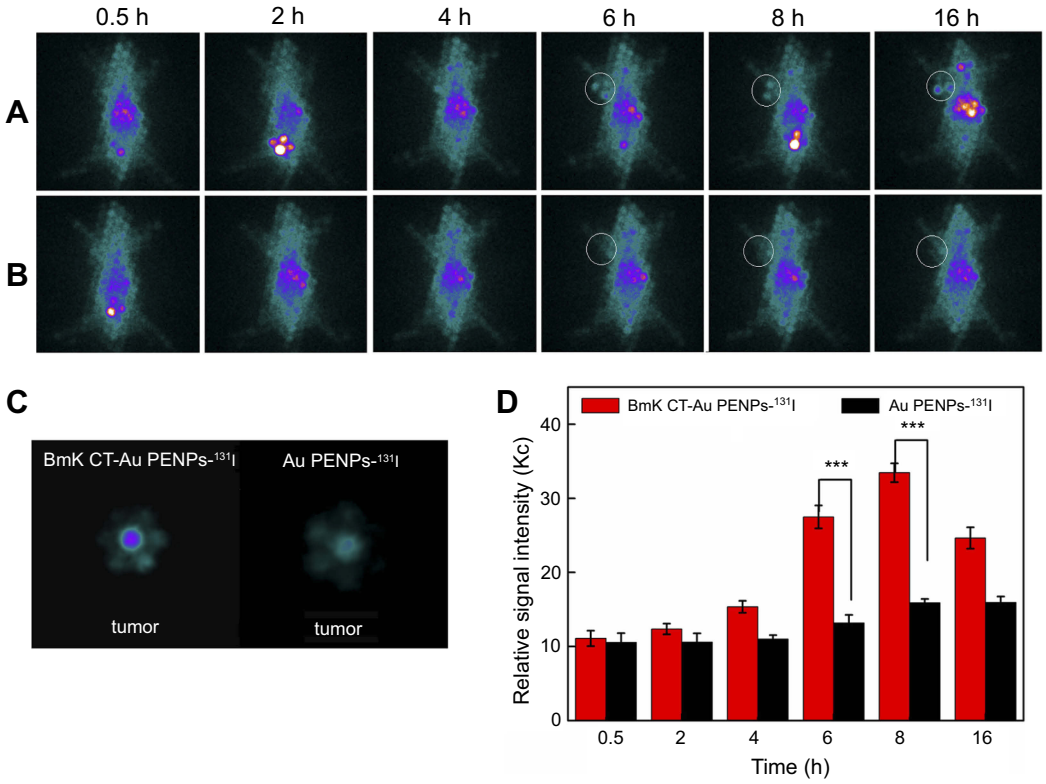

Figure 4 SPECT imaging of BmK CT-Au PENPs-^{131}I and Au PENPs-^{131}I in vivo. SPECT images of C6 tumor-bearing nude mice treated with (**A**) BmK CT-Au PENPs-^{131}I and (**B**) Au PENPs-^{131}I at different time points, and (**C**) SPECT images of ex vivo tumors at 8 hours post-injection. (**D**) The tumor relative signal intensities at different time points. The white circle denotes the tumor site. ***p<0.001

Abbreviations: SPECT, single-photon emission computed tomography; BmK CT, Buthus martensii Karsch chlorotoxin; BmK CT-Au PENPs-^{131}I, ^{131}I-labeled BmK CT modified polyethylenimine-entrapped gold nanoparticles; Au PENPs-^{131}I, ^{131}I-labeled polyethylenimine-entrapped gold nanoparticles.

higher relative SPECT signal intensity in the mice treated with BmK CT-Au PENPs-^{131}I (Figure 4C). Quantitative analysis (Figure 4D) showed that relative SPECT signal intensities in the two groups peaked at 8 hours post-injection and decreased by 16 hours post-injection, correlating with imaging results. The relative SPECT signal intensity of the BmK CT-Au PENPs-^{131}I group was higher than that of the Au PENPs-^{131}I group at the same time points. For instance, the mice treated with BmK CT-Au PENPs-^{131}I had 2.08 and 2.11 times higher tumor signal intensities than those treated with Au PENPs-^{131}I at 6 and 8 hours post-injection, respectively. In addition, biodistribution analysis was also performed to assess differences in tumor SPECT signal intensity between the BmK CT-Au PENPs-^{131}I and Au PENPs-^{131}I groups at 8 hours post-injection. As shown in Figure S6, ^{131}I-labeled Au NPs were mainly absorbed by the liver, stomach, and intestines, with relatively low radioactivity in other organs. In contrast, much higher tumor uptake of BmK CT-Au PENPs-^{131}I was observed compared with that of Au PENPs-^{131}I, further demonstrating BmK CT-dependent enhancement of tumor uptake.

Due to the targeting ability of BmK CT, similar results were observed in CT imaging of BmK CT-Au PENPs in tumor-bearing nude mice. As shown in the Figure 5A and B, the anatomic structure of implanted tumors in mice could be seen in the CT images of both the BmK CT-Au PENPs and Au PENPs groups before injection. Peak tumor CT values were observed at 8 hours post-injection, followed by a gradual decrease in mice treated with BmK CT-Au PENPs and Au PENPs. Quantitative results showed higher CT tumor values in the BmK CT-Au PENPs group during the study period (Figure 5C). In particular, the HU value of tumors in the mice treated with the BmK CT-Au PENPs was 1.67 times higher than that in mice treated with the Au PENPs at 8 hours post-injection. According to SPECT and CT data, prepared BmK CT-Au PENPs possessed targeting specificity to gliomas in vivo and could be used as a nanoprobe for SPECT/CT imaging.

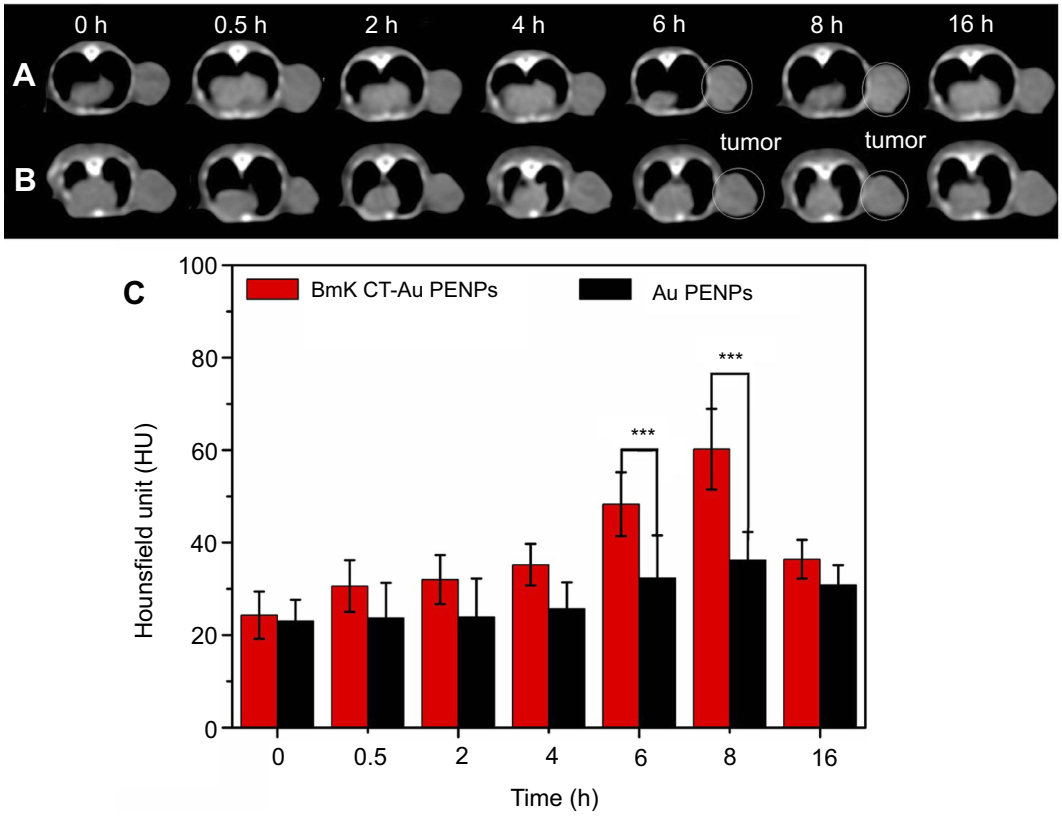

Figure 5 CT imaging of BmK CT-Au PENPs and Au PENPs in vivo. CT images of the C6 tumor-bearing nude mice before and after treatment with (**A**) BmK CT-Au PENPs and (**B**) Au PENPs, and (**C**) tumor CT values at different time points. The white circle denotes the tumor site. ***$p<0.001$

Abbreviations: CT, computed tomography; BmK CT, Buthus martensii Karsch chlorotoxin; BmK CT-Au PENPs, BmK CT modified polyethylenimine-entrapped gold nanoparticles; Au PENPs, polyethylenimine-entrapped gold nanoparticles.

Radionuclide therapy of gliomas in vivo

The targeting ability of BmK CT and properties of ^{131}I enabled BmK CT-Au PENPs-^{131}I to be used for tumor-targeted radionuclide therapy were evaluated in tumor-bearing nude mice in this study. No significant differences were observed among the control groups, which included Au PENPs-^{131}I, BmK CT-Au PENPs, Au PENPs, and saline ($p>0.05$), while BmK CT-Au PENPs-^{131}I treatment significantly inhibited tumor growth (Figure 6A). After seven treatments across 3 weeks, tumor volumes of mice in the control groups increased to levels 19.88±1.45 (Au PENPs-^{131}I), 18.99 ±2.97 (BmK CT-Au PENPs), 16.87±1.27 (Au PENPs), and 21.91±4.06 (saline) times higher than prior to treatment, whereas tumors treated with BmK CT-Au PENPs-^{131}I increased to levels 7.36±1.37 times higher than before treatment. These data demonstrated the therapeutic effects of BmK CT-Au PENPs-^{131}I in vivo. This efficacy was attributed to prolonged circulation time in vivo and delayed clearance from tumor tissues.

Survival rates of tumor-bearing mice agreed with the in vivo antitumor results (Figure 6B). These results showed that mice treated with BmK CT-Au PENPs-^{131}I had significantly longer survival time than mice in the control groups. Although the body weights among all groups were not significantly different across the 21-day treatment period (Figure S7), suggesting favorable biocompatibility of formed ^{131}I-labeled Au PENPs in vivo, all mice had died within 34 days in the control groups (Au PENPs-^{131}I [34 days], BmK CT-Au PENPs [32 days], Au PENPs [34 days], and saline [33 days]), while 25% of the mice were alive after 45 days following treatment with BmK CT-Au PENPs-^{131}I. These results revealed that the antitumor efficacy of ^{131}I-labeled Au PENPs was enhanced through modification with BmK CT.

To further evaluate therapeutic effects and safety of BmK CT-Au PENPs-^{131}I in vivo, H&E and TUNEL staining were performed. H&E staining results showed that necrotic regions were only observed in tumors treated with BmK CT-Au PENPs-^{131}I or Au PENPs-^{131}I (Figure 6C) and the necrotic

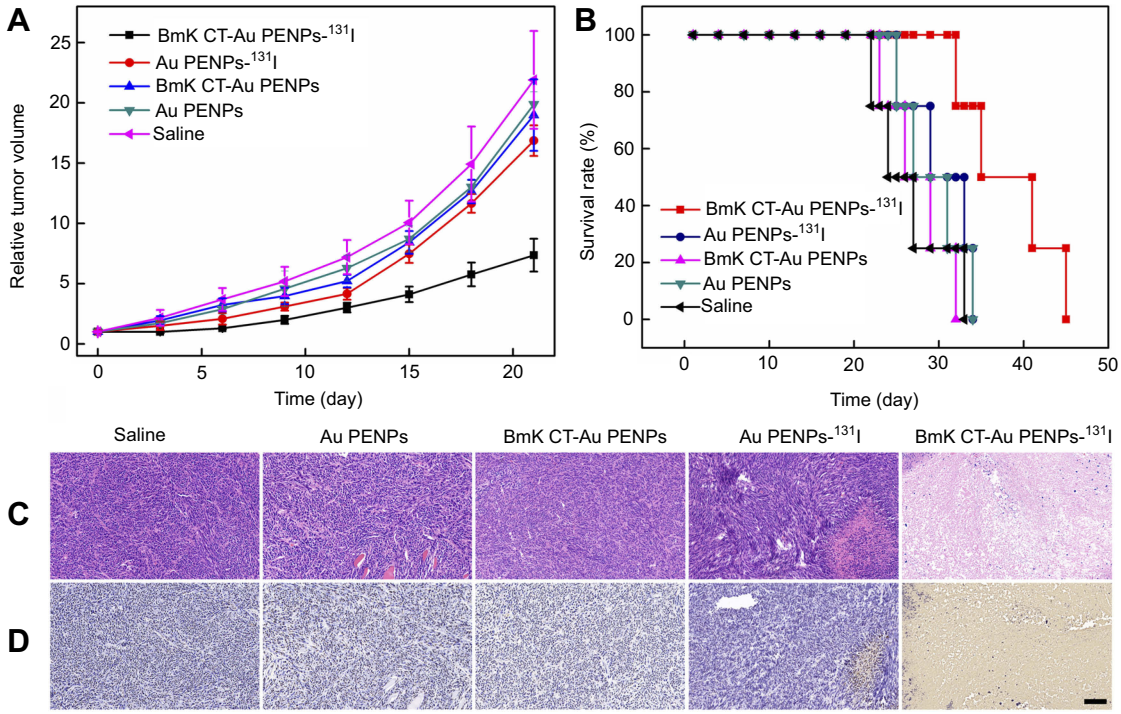

Figure 6 Tumor inhibition by BmK CT-Au PENPs-^{131}I in vivo. (**A**) Relative tumor volume of C6 tumor-bearing nude mice treated with saline, Au PENPs, BmK CT-Au PENPs, Au PENPs-^{131}I, and BmK CT-Au PENPs-^{131}I. (**B**) Survival rate, (**C**) H&E staining, and (**D**) TUNEL assay of C6 tumor-bearing mice after a 21-day treatment course (mean ± SD, n=5). The scale bar shown in both panels represents 200 μm.

Abbreviations: BmK CT, Buthus martensii Karsch chlorotoxin; BmK CT-Au PENPs, BmK CT modified polyethylenimine-entrapped gold nanoparticles; Au PENPs, polyethylenimine-entrapped gold nanoparticles; BmK CT-Au PENPs-^{131}I, ^{131}I-labeled BmK CT modified polyethylenimine-entrapped gold nanoparticles; Au PENPs-^{131}I, ^{131}I-labeled polyethylenimine-entrapped gold nanoparticles.

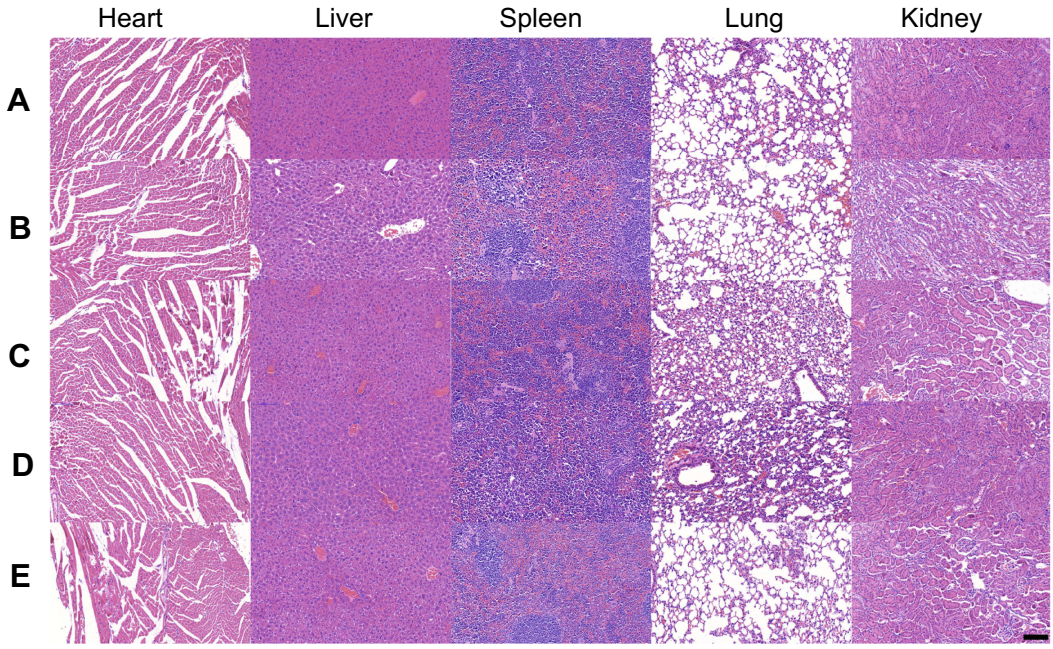

Figure 7 H&E staining of the heart, liver, spleen, lung, and kidney of the mice after the 21-day treatment of (**A**) saline, (**B**) Au PENPs, (**C**) BmK CT-Au PENPs, (**D**) Au PENPs-^{131}I, and (**E**) BmK CT-Au PENPs-^{131}I. The scale bar in each panel indicates 200 μm.

Abbreviations: BmK CT, Buthus martensii Karsch chlorotoxin; BmK CT-Au PENPs, BmK CT modified polyethylenimine-entrapped gold nanoparticles; Au PENPs, polyethylenimine-entrapped gold nanoparticles; BmK CT-Au PENPs-^{131}I, ^{131}I-labeled BmK CT modified polyethylenimine-entrapped gold nanoparticles; Au PENPs-^{131}I, ^{131}I-labeled polyethylenimine-entrapped gold nanoparticles.

area in the BmK CT-Au PENPs-^{131}I group was much larger than that in the Au PENPs-^{131}I group. A similar trend was observed in TUNEL assay results (Figure 6D). Positive staining of apoptotic cells was only observed in the tumor sections treated with Au PENPs-^{131}I or BmK CT-Au PENPs-^{131}I, and the area of apoptotic cells was much greater in the BmK CT-Au PENPs-^{131}I group. Therefore, the results of H&E and TUNEL staining confirmed that BmK CT modification enabled ^{131}I-labeled Au PENPs' targeting specificity to gliomas and enhanced the therapeutic effects on tumor cells. We further assessed potential toxicity of the multifunctional Au NPs before and after ^{131}I labeling toward major organs using H&E staining (Figure 7). No obvious organ damage or abnormalities were observed, indicating good organ compatibility of the multifunctional Au NPs before and after ^{131}I labeling.

Conclusion

In this work, we developed ^{131}I-labeled Au PENPs for tumor-targeted SPECT/CT imaging and radiotherapy. PEGylated PEI was sequentially linked with BmK CT and HPAO to be used as a template for entrapment of Au NPs. BmK CT-Au PENPs showed favorable water solubility and stability, X-ray attenuation properties, and cytocompatibility at the prepared Au concentrations. After ^{131}I radiolabeling through the HPAO on the PEI surface, BmK CT-Au PENPs-^{131}I exhibited relatively high radiochemical purity and radiostability in vitro, and were used as a multifunctional nanoprobe for targeted SPECT/CT imaging and radionuclide therapy of tumor cells in vitro and in a tumor-bearing mouse model in vivo, with acceptable organ compatibility. The synthesized multifunctional Au PENPs may hold great promise in SPECT/CT imaging and radiotherapy of different MMP2-overexpressing tumors.

Acknowledgments

The present study was financially supported by the National Natural Science Foundation of China (81671712, 81801727, 21807059, and 81301245), and Shanghai Sailing Program (16YF1409300). The synthesis and characterization of the nanoparticles in this study were performed by J Zhu through the funding from and facilities at the Nanjing Tech University. J Zhu is grateful for the support from the Natural Science Foundation of Jiangsu Province (BK20180711) and the Natural Science Foundation for Colleges and Universities in Jiangsu Province (17KJB350005).

Disclosure

The authors report no conflicts of interest in this work.

References

1. Wicki A, Witzigmann D, Balasubramanian V, Huwyler J. Nanomedicine in cancer therapy: challenges, opportunities, and clinical applications. *J Control Release*. 2015;200:138–157. doi:10.1016/j.jconrel.2014.12.030
2. Shi J, Kantoff PW, Wooster R, Farokhzad OC. Cancer nanomedicine: progress, challenges and opportunities. *Nat Rev Cancer*. 2016;17(1):20–37. doi:10.1038/nrc.2016.108
3. Bush NAO, Chang SM, Berger MS. Current and future strategies for treatment of glioma. *Neurosurg Rev*. 2017;40(1):1–14. doi:10.1007/s10143-016-0709-8
4. Chaichana KL, Jusue-Torres I, Lemos AM, et al. The butterfly effect on glioblastoma: is volumetric extent of resection more effective than biopsy for these tumors? *J Neurooncol*. 2014;120(3):625–634. doi:10.1007/s11060-014-1597-9
5. Chaichana KL, Jusue-Torres I, Navarro-Ramirez R, et al. Establishing percent resection and residual volume thresholds affecting survival and recurrence for patients with newly diagnosed intracranial glioblastoma. *Neuro Oncol*. 2014;16(1):113–122. doi:10.1093/neuonc/not137
6. Gallego O. Nonsurgical treatment of recurrent glioblastoma. *Curr Oncol*. 2015;22(4):9. doi:10.3747/co.22.2368
7. Chen X, Gambhir SS, Cheon J. Theranostic nanomedicine. *Acc Chem Res*. 2011;44(10):841. doi:10.1021/ar200231d
8. Signore A, Glaudemans AWJM. The molecular imaging approach to image infections and inflammation by nuclear medicine techniques. *Ann Nucl Med*. 2011;25(10):681–700. doi:10.1007/s12149-011-0521-z
9. Gomes CM, Abrunhosa AJ, Ramos P, Pauwels EKJ. Molecular imaging with SPECT as a tool for drug development. *Adv Drug Deliv Rev*. 2011;63(7):547–554. doi:10.1016/j.addr.2010.09.015
10. Ametamey SM, Honer M, Schubiger PA. Molecular imaging with PET. *Chem Rev*. 2008;108(5):1501–1516. doi:10.1021/cr0782426
11. Xing Y, Zhu J, Zhao L, et al. SPECT/CT imaging of chemotherapy-induced tumor apoptosis using ^{99m}Tc-labeled dendrimer-entrapped gold nanoparticles. *Drug Deliv*. 2018;25(1):1384–1393. doi:10.1080/10717544.2018.1474968
12. Rainone P, Riva B, Belloli S, et al. Development of ^{99m}Tc-radiolabeled nanosilica for targeted detection of HER2-positive breast cancer. *Int J Nanomedicine*. 2017;12:3447–3461. doi:10.2147/IJN.S129720
13. Chrastina A, Schnitzer JE. Iodine-125 radiolabeling of silver nanoparticles for *in vivo* SPECT imaging. *Int J Nanomedicine*. 2010;5:653–659. doi:10.2147/IJN.S11677
14. Rangger C, Helbok A, Sosabowski J, et al. Tumor targeting and imaging with dual-peptide conjugated multifunctional liposomal nanoparticles. *Int J Nanomedicine*. 2013;8:4659–4671.
15. Tsai C-C, Chang C-H, Chen L-C, et al. Biodistribution and pharmacokinetics of 188Re-liposomes and their comparative therapeutic efficacy with 5-fluorouracil in C26 colonic peritoneal carcinomatosis mice. *Int J Nanomedicine*. 2011;6:2607–2619.
16. Zhao L, Zhu M, Li Y, et al. Radiolabeled dendrimers for nuclear medicine applications. *Molecules*. 2017;22(9):1350. doi:10.3390/molecules22091350
17. Zhao L, Zhu J, Cheng Y, et al. Chlorotoxin-conjugated multifunctional dendrimers labeled with radionuclide ^{131}I for single photon emission computed tomography imaging and radiotherapy of gliomas. *ACS Appl Mater Interfaces*. 2015;7(35):19798–19808. doi:10.1021/acsami.5b05836
18. Kozempel J, Vlk M, Málková E, et al. Prospective carriers of ^{223}Ra for targeted alpha particle therapy. *J Radioanal Nucl Chem*. 2015;304(1):443–447. doi:10.1007/s10967-014-3615-y

19. Toro-González M, Copping R, Mirzadeh S, Rojas JV. Multifunctional $GdVO_4$: Eu core–shell nanoparticles containing ^{225}Ac for targeted alpha therapy and molecular imaging. *J Mater Chem B*. 2018;6(47):7985–7997. doi:10.1039/C8TB02173B
20. Westrøm S, Malenge M, Jorstad IS, et al. Ra-224 labeling of calcium carbonate microparticles for internal α-therapy: preparation, stability, and biodistribution in mice. *J Labelled Comp Radiopharm*. 2018;61(6):472–486. doi:10.1002/jlcr.3610
21. Mokhodoeva O, Vlk M, Málková E, et al. Study of ^{223}Ra uptake mechanism by Fe_3O_4 nanoparticles: towards new prospective theranostic SPIONs. *J Nanopart Res*. 2016;18(10):301. doi:10.1007/s11051-016-3615-7
22. Chen L, Zhong X, Yi X, et al. Radionuclide ^{131}I labeled reduced graphene oxide for nuclear imaging guided combined radio- and photothermal therapy of cancer. *Biomaterials*. 2015;66:21–28. doi:10.1016/j.biomaterials.2015.06.043
23. Zhang Y, Zhang Y, Yin L, et al. Synthesis and bioevaluation of iodine-131 directly labeled cyclic rgd-pegylated gold nanorods for tumor-targeted imaging. *Contrast Media Mol Imaging*. 2017;2017:6081724. doi:10.1155/2017/6081724
24. Huang P, Zhang Y, Wang W, et al. Co-delivery of doxorubicin and ^{131}I by thermosensitive micellar-hydrogel for enhanced in situ synergetic chemoradiotherapy. *J Control Release*. 2015;220:456–464. doi:10.1016/j.jconrel.2015.11.007
25. Liu K, Zheng D, Zhao J, et al. pH-sensitive nanogels based on the electrostatic self-assembly of radionuclide ^{131}I labeled albumin and carboxymethyl cellulose for synergistic combined chemo-radioisotope therapy of cancer. *J Mater Chem B*. 2018;6(29):4738–4746. doi:10.1039/C8TB01295D
26. Zhong X, Yang K, Dong Z, et al. Polydopamine as a biocompatible multifunctional nanocarrier for combined radioisotope therapy and chemotherapy of cancer. *Adv Funct Mater*. 2015;25(47):7327–7336. doi:10.1002/adfm.201503587
27. Li Z, Wang B, Zhang Z, et al. Radionuclide imaging-guided chemo-radioisotope synergistic therapy using a ^{131}I-labeled polydopamine multifunctional nanocarrier. *Mol Ther*. 2018;26(5):1385–1393. doi:10.1016/j.ymthe.2018.02.019
28. Qiao W, Zhao L, Wu S, et al. SPECT imaging and radionuclide therapy of glioma using ^{131}I labeled Buthus martensii Karsch chlorotoxin. *J Neurooncol*. 2017;133(2):287–295. doi:10.1007/s11060-017-2456-2
29. Cheng Y, Zhu J, Zhao L, et al. ^{131}I-labeled multifunctional dendrimers modified with BmK CT for targeted SPECT imaging and radiotherapy of gliomas. *Nanomedicine (Lond)*. 2016;11(10):1253–1266. doi:10.2217/nnm-2016-0001
30. Mamelak AN, Rosenfeld S, Bucholz R, et al. Phase I single-dose study of intracavitary-administered iodine-131-TM-601 in adults with recurrent high-grade glioma. *J Clin Oncol*. 2006;24(22):3644–3650. doi:10.1200/JCO.2005.05.4569
31. Cohen-Inbar O, Zaaroor M. Glioblastoma multiforme targeted therapy: the Chlorotoxin story. *J Clin Neurosci*. 2016;33:52–58. doi:10.1016/j.jocn.2016.04.012
32. Krolicki L, Bruchertseifer F, Kunikowska J, et al. Prolonged survival in secondary glioblastoma following local injection of targeted alpha therapy with ^{213}Bi-substance P analogue. *Eur J Nucl Med Mol Imaging*. 2018;45(9):1636–1644. doi:10.1007/s00259-018-4015-2
33. Hallouard F, Anton N, Choquet P, Constantinesco A, Vandamme T. Iodinated blood pool contrast media for preclinical X-ray imaging applications – a review. *Biomaterials*. 2010;31(24):6249–6268. doi:10.1016/j.biomaterials.2010.04.066
34. Qin J, Peng C, Zhao B, et al. Noninvasive detection of macrophages in atherosclerotic lesions by computed tomography enhanced with PEGylated gold nanoparticles. *Int J Nanomedicine*. 2014;9:5575–5590. doi:10.2147/IJN.S72819
35. Day ES, Bickford LR, Slater JH, Riggall NS, Drezek RA, West JL. Antibody-conjugated gold-gold sulfide nanoparticles as multifunctional agents for imaging and therapy of breast cancer. *Int J Nanomedicine*. 2010;5:445–454.
36. Guo J, Rahme K, He Y, Li L-L, Holmes JD, O'Driscoll CM. Gold nanoparticles enlighten the future of cancer theranostics. *Int J Nanomedicine*. 2017;12:6131–6152. doi:10.2147/IJN.S140772
37. Popovtzer R, Agrawal A, Kotov NA, et al. Targeted gold nanoparticles enable molecular CT imaging of cancer. *Nano Lett*. 2008;8(12):4593–4596.
38. Zhou B, Zheng L, Peng C, et al. Synthesis and characterization of pegylated polyethylenimine-entrapped gold nanoparticles for blood pool and tumor CT imaging. *ACS Appl Mater Interfaces*. 2014;6(19):17190–17199. doi:10.1021/am505006z
39. Zhu J, Sun W, Zhang J, et al. Facile formation of gold-nanoparticle-loaded γ-polyglutamic acid nanogels for tumor computed tomography imaging. *Bioconjug Chem*. 2017;28(11):2692–2697. doi:10.1021/acs.bioconjchem.7b00571
40. Muddineti OS, Ghosh B, Biswas S. Current trends in using polymer coated gold nanoparticles for cancer therapy. *Int J Pharm*. 2015;484(1):252–267. doi:10.1016/j.ijpharm.2015.02.038
41. Zhou B, Zhao L, Shen M, Zhao J, Shi X. A multifunctional polyethylenimine-based nanoplatform for targeted anticancer drug delivery to tumors. *In Vivo J Mater Chem B*. 2017;5(8):1542–1550. doi:10.1039/C6TB02620F
42. Zhao M-D, Cheng J-L, Yan J-J, et al. Hyaluronic acid reagent functional chitosan-PEI conjugate with AQP2-siRNA suppressed endometriotic lesion formation. *Int J Nanomedicine*. 2016;11:1323–1336. doi:10.2147/IJN.S99692
43. Li J-M, Zhang W, Su H, et al. Reversal of multidrug resistance in MCF-7/Adr cells by codelivery of doxorubicin and BCL2 siRNA using a folic acid-conjugated polyethylenimine hydroxypropyl-β-cyclodextrin nanocarrier. *Int J Nanomedicine*. 2015;10:3147–3162. doi:10.2147/IJN.S67146
44. Zhuang Y, Zhao L, Zheng L, et al. Laponite-polyethylenimine based theranostic nanoplatform for tumor-targeting CT imaging and chemotherapy. *ACS Biomater Sci Eng*. 2017;3(3):431–442. doi:10.1021/acsbiomaterials.6b00528
45. Zhou B, Wang R, Chen F, et al. ^{99m}Tc-labeled RGD-polyethylenimine conjugates with entrapped gold nanoparticles in the cavities for dual-mode SPECT/CT imaging of hepatic carcinoma. *ACS Appl Mater Interfaces*. 2018;10(7):6146–6154. doi:10.1021/acsami.7b17107
46. Zhao L, Wen S, Zhu M, et al. ^{99m}Tc-labelled multifunctional polyethylenimine-entrapped gold nanoparticles for dual mode SPECT and CT imaging. *Artif Cells Nanomed Biotechnol*. 2018;46(sup1):488–498. doi:10.1080/21691401.2018.1430696